inorganics

MDPI

Article

Ti_3AlC_2 MAX/MXene for Hydrogen Generation via Photocatalytic Hydride Hydrolysis

Hani Nasser Abdelhamid

Department of Chemistry, College of Science, Imam Mohammad Ibn Saud Islamic University (IMSIU), Riyadh 11623, Saudi Arabia; hnabdelhamid@imamu.edu.sa or hani.nasserabdelhamid@gmail.com

Abstract: Reducing dehydrogenation temperature while preserving high hydrogen generation capacity obstructs the hydrolysis of sodium borohydrides ($NaBH_4$). The two-dimensional (2D) MAX phase of titanium aluminum carbide (Ti_3AlC_2) and MXene ($Ti_3C_2T_x$) multilayers was investigated for hydrogen generation via $NaBH_4$ hydrolysis with and without light. The material was characterized using X-ray diffraction (XRD), Fourier transform infrared (FT-IR), transmission electron microscopy (TEM), high-resolution TEM (HR-TEM), scanning electron microscopy (SEM), and diffuse reflectance spectroscopy (DRS). The activity of Ti_3AlC_2 was significantly enhanced by the integration of UV light radiation during hydrolysis. $Ti_3AlC_2/Ti_3C_2T_x$ improved the dehydrogenation rates of $NaBH_4$ at ambient conditions and maintained high hydrogen generation rates (HGRs) over time compared to a conventional method. It exhibited a HGR of 200–300 $mL{\cdot}min^{-1}{\cdot}g^{-1}$. Photo-assisted hydrolysis over the catalyst can be maintained for several times at ambient temperature. The catalyst demonstrated effective performance even after five cycles of usage.

Keywords: MXene; hydrogen generation; hydrides; photocatalysis; $NaBH_4$

1. Introduction

Hydrogen gas has been considered the fuel of the future [1,2]. It can be produced via several methods for hydrogen generation, such as photocatalysis [3–5], electrolysis [6–8], biological production [9], dehydrogenation of a molecule [10], and reforming of fossil fuels [11]. In general, they can classified into three common approaches: (1) thermal-based method (e.g., reforming natural gas), (2) electrolytic-based method (e.g., water electrolysis); and (3) photolytic-based method (e.g., photobiological, photoelectrochemical, and photocatalytic) [12]. However, mixed strategies were also reported, e.g., the photoelectrochemical method, which included photocatalysis and electrolysis simultaneously. Hydrogen storage is the second obstacle for the hydrogen economy after production. Hydrogen can be stored in the gas phase as a compressed gas in tanks, liquids, or solid states. Metal hydrides are promising solid-state hydrogen storage materials [13]. They offered advantages of high hydrogen capacity, require low storage pressure, and exhibit high reversibility [14,15].

MXene materials are two-dimensional (2D) metal of nitrides, carbides, or carbonitrides [16]. They have a standard formula of $M_{n+1}X_nT_x$ (where X denotes N or C, M represents a transition metal, n equals 1-3, and T_x is surface functional groups) [17]. They are synthesized by removing the interlayer of the MAX phase. They demonstrated significant potential for various applications, including supercapacitors, photocatalysis, solar batteries, and batteries [17,18]. Among MXene materials, titanium carbide (Ti_3C_2) is the prototypical and most extensively studied material, and it is noted for its abundant surface active sites, high stability, and good electrical conductivity [19].

check for updates

Academic Editor: Torben R. Jensen

Received: 12 January 2025
Revised: 31 January 2025
Accepted: 3 February 2025
Published: 5 February 2025

Citation: Abdelhamid, H.N. Ti_3AlC_2 MAX/MXene for Hydrogen Generation via Photocatalytic Hydride Hydrolysis. *Inorganics* **2025**, *13*, 44. https://doi.org/10.3390/inorganics13020044

Copyright: © 2025 by the author. Licensee MDPI, Basel, Switzerland. This article is an open access article distributed under the terms and conditions of the Creative Commons Attribution (CC BY) license (https://creativecommons.org/licenses/by/4.0/).

Mxene-based photocatalysts are promising for hydrogen generation via several approaches, including photocatalysis [3,20], electrocatalysis [21,22], the photoelectrochemical method [23], methane dry reforming [24], and the dehydrogenation of hydrides [25]. Thus, 2D MAX/MXene of the Ti_3AlC_2 monolayer and multilayers were integrated with titanium dioxide (TiO_2) [26], TiO_2/Ni_2P [27], PtO/TiO_2 [28], 1D/2D CdS [29,30], $CdS/g\text{-}C_3N_4$ [31], $SrTiO_3/g\text{-}C_3N_4$ [32], metal-organic frameworks (MOFs) [33], and TiO_2/MOF [34], forming heterojunctions for photocatalytic hydrogen production. They can serve as cocatalysts to improve the photocatalytic hydrogen generation of TiO_2 [35]. The photocatalytic performance of MXene-based photocatalysts can be enhanced by adding noble metals [36].

Mxene also offered promising properties as a hydrogen storage material and hydrogen production from chemicals via conversion. Multilayer $Ti_3C_2T_x$ MXene showed 10.47 wt.% of hydrogen storage at 25 bar and 77 K [37]. VF_4/Ti_3C_2 improved the hydrogen storage process of $Mg(BH_4)_2$ [38]. The palladium (Pd)@MXene showed high catalytic performance in the hydrolysis of methylamine-borane (CH_3NH_2–BH_3, MeAB) with a hydrogen generation rate of 159.4 min^{-1} at 318 K [39]. The $Pd@Ti_3AlC_2$ composite showed hydrogen generation from alkaline formaldehyde [40]. Pd@alkalized Ti_3C_2 (alk-Ti_3C_2) [41], $Ru/Ti_3C_{2-x}N_x$ [42], $Pt/Ti_3C_2T_x$ [43], and 2D bimetallic $Pt_yCo_{1-y}/Ti_3C_2X_2$ [44] were reported for the hydrolysis of ammonia borane (AB). NiPt/TiO_2-decorated $Ti_3C_2T_x$ was reported to show hydrogen generation from hydrazine [45]. Noble metal enhanced the hydrolysis of hydrogen storage materials [46]. The photocatalytic dehydrogenation of hydrides is very limited.

Herein, the titanium aluminum carbide (Ti_3AlC_2) MAX phase with and without light were investigated for sodium borohydride ($NaBH_4$) hydrolysis and hydrogen generation. The materials were characterized using X-ray diffraction (XRD), Fourier transform infrared (FT-IR), diffuse reflectance spectroscopy (DRS), Tauc's plot, scanning electron microscopy (SEM), transmission electron microscopy (TEM), and high-resolution TEM (HR-TEM) images. UV light radiation enhanced hydrolysis in continuous high hydrogen generation rates (HGRs) compared to conventional hydrolysis (without light).

2. Results and Discussion

2.1. Characterization

Ti_3AlC_2 MAX materials exhibit layers of Ti-C separated with aluminum ions (Figure 1). The delamination of the material includes chemical etching using HF to remove the aluminum between the layers [47]. The material properties were identified using XRD (Figure 2a), FT-IR (Figure 2b), DRS (Figure 3a), Tauc's plot (Figure 3b), SEM images (Figure 4a–d), TEM and HR-TEM images (Figure 5a,b).

The material crystallinity and phase purity were assessed using XRD patterns (Figure 2a). The simulated XRD pattern from JCPDS No. 52–0875 agrees with the pattern for Ti_3AlC_2. The XRD patterns of layered Ti_3AlC_2 exhibit distinct peaks at 2θ values of 9.4°, 19.1°, 33.6°, 36.6°, 38.8°, 41.5°, 44.6°, 48.1°, 52.4°, 56.5°, 60.3°, 65.5°, 72.4°, and 74.5°, corresponding to the Miller indexes of (002), (101), (103), (104), (105), (106), (107), and (108), of pristine Ti_3AlC_2, respectively. The diffraction peaks for Ti_3AlC_2 at 38.8–41.5° reveals a high degree of crystallinity (Figure 2a). HF-etching causes removing Al-layer offering multilayers of $Ti_3C_2T_x$ (Figure 1).

The chemical bond and connectivity within the materials were evaluated using the FT-IR spectrum (Figure 2b). Data analysis of the FT-IR spectrum of Ti_3AlC_2 identifies the functional groups within the wavenumber range of 400–1000 cm^{-1} (Figure 2b). Al–O, Ti–O, and Ti–C vibrational modes are shown in the 400–600 cm^{-1} range (Figure 2b).

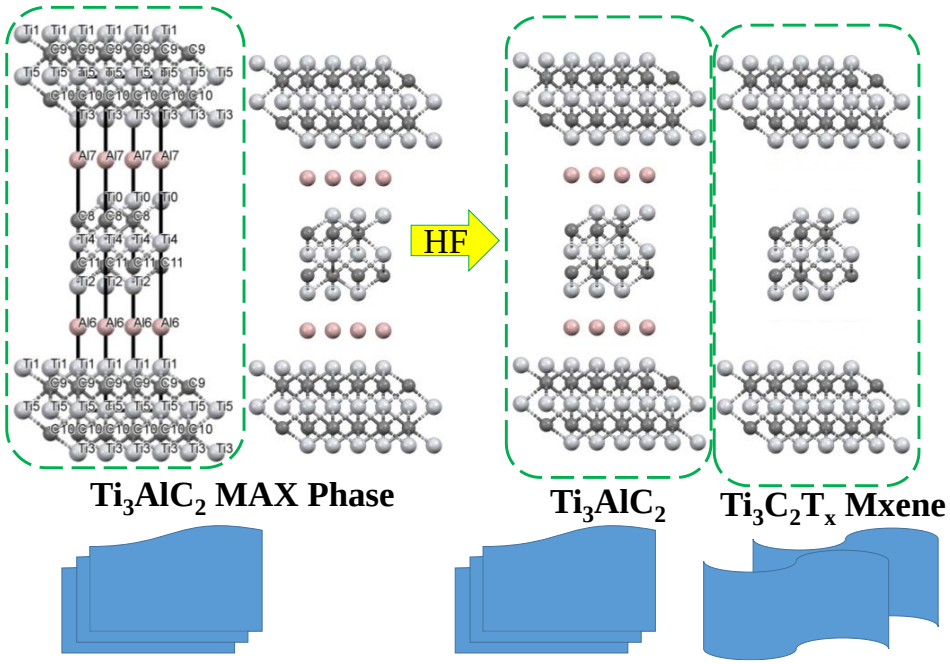


Figure 1. Chemical etching of Ti_3AlC_2 MAX phase.

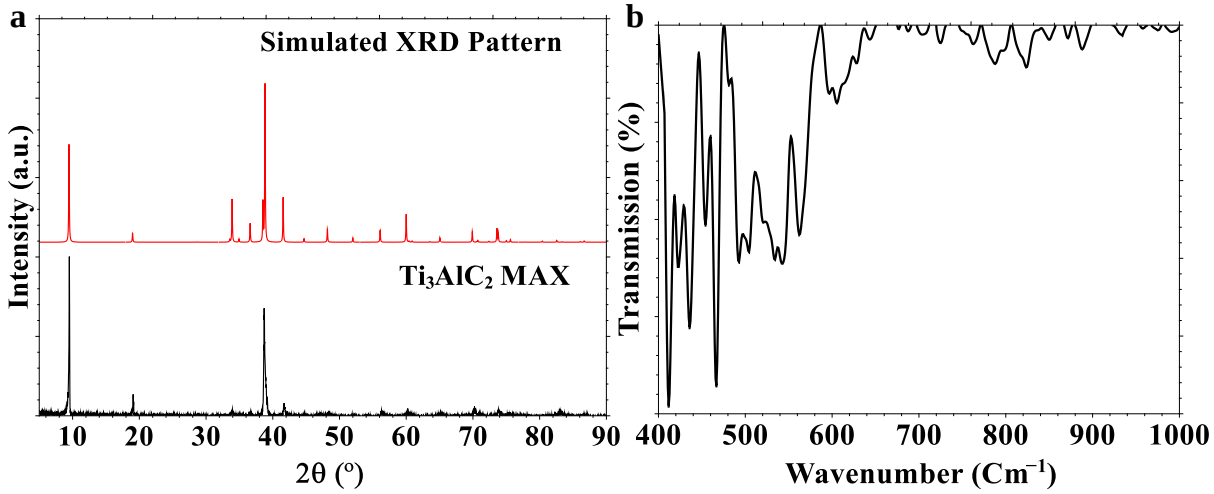


Figure 2. Characterization of the materials using (**a**) XRD for synthesized and simulated patterns of Ti_3AlC_2 material and (**b**) FT-IR.

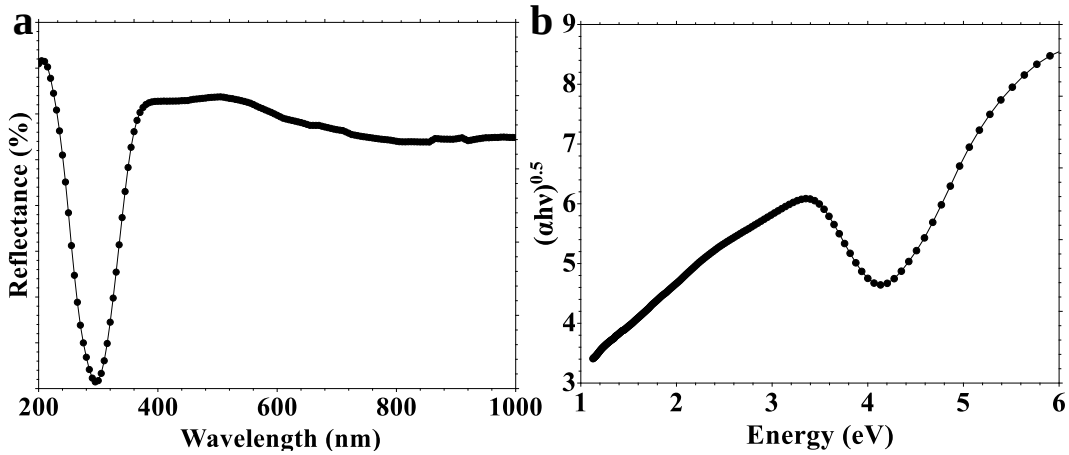


Figure 3. (**a**) DRS and (**b**) Tauc's plots of prepared materials.

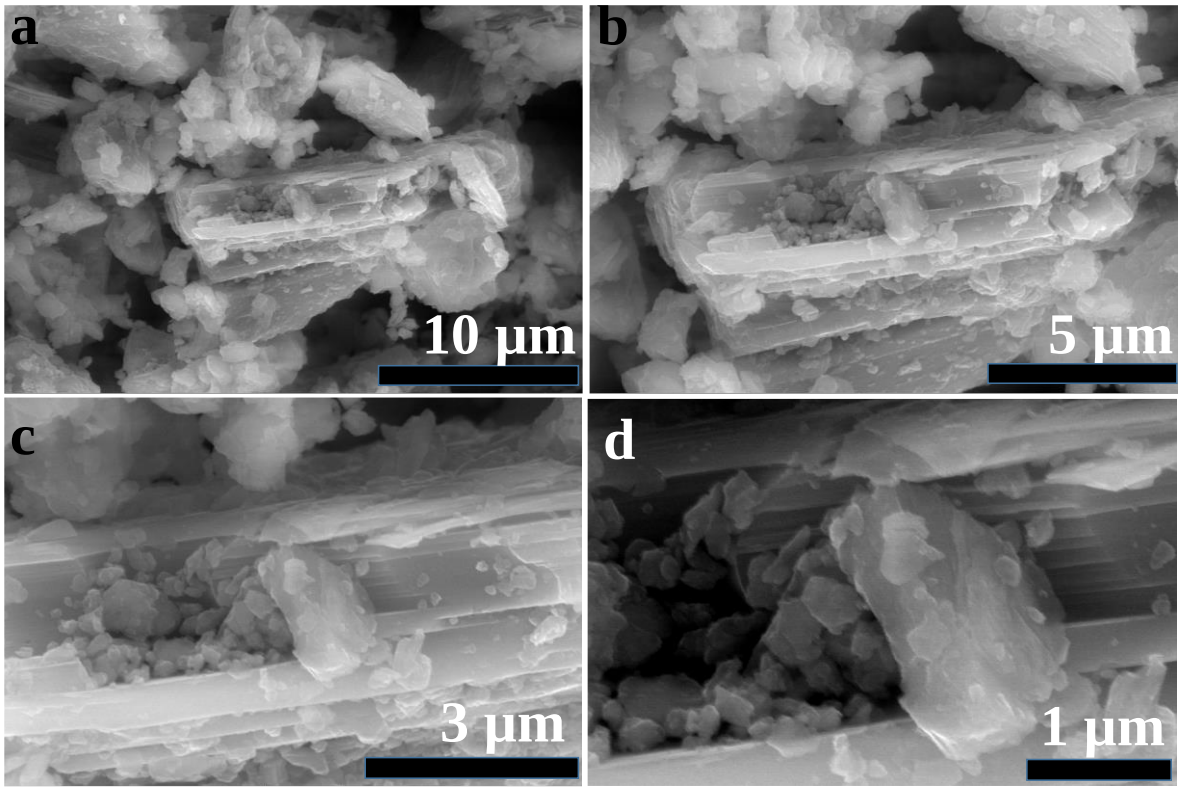


Figure 4. (**a**–**d**) SEM images of Ti_3AlC_2 in different magnifications.

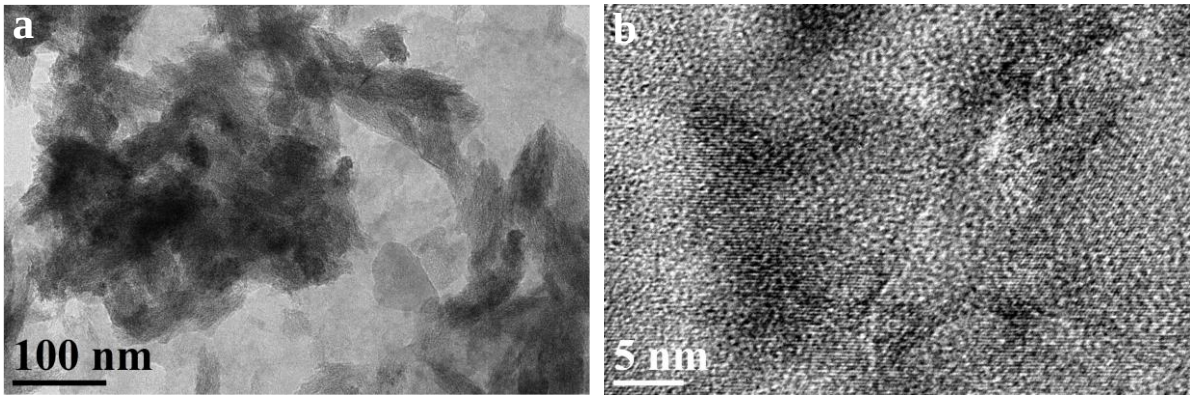


Figure 5. (**a**) TEM and (**b**) HR-TEM image of the material.

The optical properties of Ti_3AlC_2 were evaluated using DRS (Figure 3a) and Tauc's plot (Figure 3b). There is no reflectance in the range of 400–1000 nm. On the other side, a strong reflectance was observed at 295 nm, corresponding to a bandgap of 4.2 eV using the equation of 1240/λ, where λ is the wavelength in nm, i.e., 295 nm (Figure 3b). Typical DRS values of Ti_3AlC_2 show no reflectance in this range. The observed reflectance could be due to the oxidation of $Ti_3C_2T_x$ nanosheets into TiO_2 [48,49].

Figure 4 illustrates the morphology of Ti_3AlC_2 as analyzed by SEM. Figure 4 illustrates the layered structure of Ti_3AlC_2. According to the SEM images of Ti_3AlC_2, the images distinctly illustrate the plate-like shape of the Ti_3AlC_2 particles. This observation is a distinctive attribute of MAX phase materials. The particles exhibit minor agglomeration, resulting in the formation of clusters. SEM images show a broad size distribution with a diverse range of dimensions from a few micrometers to several hundred nanometers. These observations indicate that the synthesis procedure may have produced a heterogeneous

particle population. SEM analysis can be used to assess the topographical properties of the materials. The particle surfaces exhibit an exceptionally smooth texture. The particles exhibit interlocking behavior in certain regions, potentially enhancing the material's mechanical capabilities. The SEM images indicate that the Ti_3AlC_2 material has a plate-like shape characterized by a broad size distribution and generally smooth surfaces.

To comprehensively understand the Ti_3AlC_2 material, a supplementary characterization procedure was performed using TEM (Figure 5a) and HR-TEM images (Figure 5b). TEM image depicts dark regions associated with compact stacked Ti_3AlC_2 (Figure 5a). However, there are also transparent objects for monolayers or a few layers of MXene materials. The particles are mildly agglomerated, creating clusters. This observation aligns with the SEM observations (Figure 4). The particles display a broad spectrum of dimensions, ranging from 50 to 200 nm. The HR-TEM image offers an enhanced resolution perspective of the material's architecture (Figure 5b). Although the overall image seems amorphous, several areas exhibit lattice fringes, indicating the existence of nanocrystalline domains (Figure 5b).

The lattice fringes may indicate the interplanar spacing of the crystal structure. Figure 5b illustrates the interplanar distance, which is predicted to be 0.21 nm. The TEM and HR-TEM images suggest that the crystalline material confirms the XRD pattern (Figure 2).

2.2. Hydrogen Generation

Metal hydrides are promising as hydrogen storage materials. There are several metal hydrides. Among these types, $NaBH_4$ is a renewable hydrogen storage material due to its high hydrogen capacitance of 10.6 wt.%. The hydrogen generated from $NaBH_4$ via hydrolysis can be illustrated as $NaBH_4 + (2 + x)H_2O \rightarrow 4H_2 + NaBO_2 \cdot xH_2O$. This equation reveals that 50% of hydrogen is from $NaBH_4$, while the other 50% comes from water molecules. The hydrolysis of $NaBH_4$ was catalyzed using the synthesized material without and with light (Figure 6).

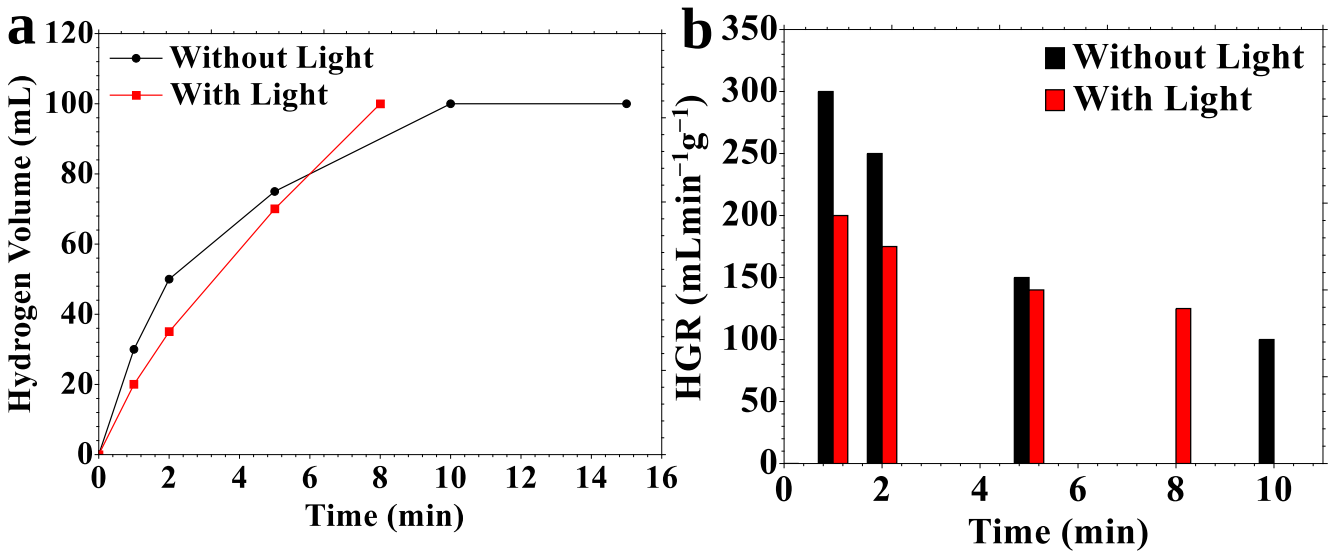


Figure 6. (**a**) Hydrogen volume over time and (**b**) HGR over time for $NaBH_4$ hydrolysis with and without light.

Hydrogen generation from $NaBH_4$ hydrolysis is shown in Figure 6. The black line illustrates hydrogen evolution without illumination (Figure 6a). The volume of hydrogen increases consistently with time, attaining a plateau after roughly 10 min (Figure 6a). The hydrogen evolution was also recorded under illumination (Figure 6a). The hydrogen

volume increased with a markedly accelerated rate relative to the dark situation, attaining a superior plateau value (Figure 6a).

The hydrogen generation rate (HGR) was plotted for experiments with and without light, as shown in Figure 6b. The y-axis denotes the HGR, defined as the hydrogen volume generated per unit time per unit mass of catalyst ($mL \cdot min^{-1} \cdot g^{-1}$). In the absence of light, the HGR is initially elevated but diminishes swiftly over time. Meanwhile, in the presence of light, the HGR regularly exceeds that of the dark state, signifying a substantial increase in hydrogen generation. The data unequivocally indicate that light substantially improves hydrogen evolution. This observation is demonstrated by the high hydrogen volume generated and the high HGR noted in the presence of light. The increased hydrogen production under light is due to the material's photocatalytic activity. Light can energize electrons within the material, resulting in the formation of electron-hole pairs. Figure 6 presents evidence of the material's photocatalytic activity and capacity to increase hydrogen production under lighting.

The recyclability of the catalyst is an essential aspect of industrial concerns. The catalytic performance of the catalyst was recycled for five cycles with and without light, as shown in Figure 7. The volume of hydrogen generated in each cycle exhibits insignificant fluctuations. This observation may result from differences in catalyst activity, reaction conditions, or reagent contaminants. There is no reduction in hydrogen generation regarding the quantity of hydrogen created. There is solely an increase in the duration needed to attain the maximum amount of hydrogen produced. The catalyst's inherent activity is likely unaffected by repeated utilization (Figure 7). The data demonstrate that Ti_3AlC_2 is suitable for multiple cycles of hydrogen production via $NaBH_4$ hydrolysis.

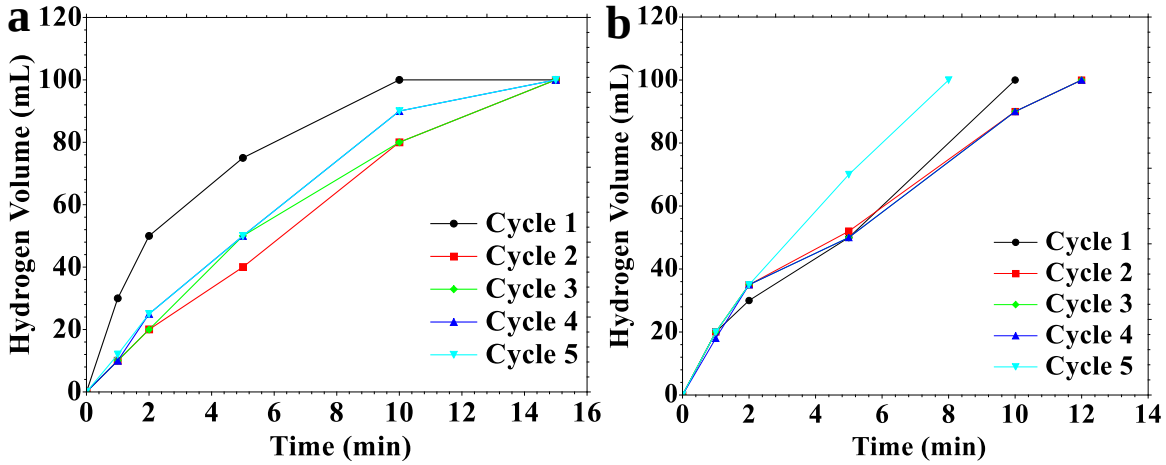


Figure 7. Recyclability for $NaBH_4$ hydrolysis using Ti_3AlC_2 MAX/Mxene (**a**) without and (**b**) with light radiation.

A summary of hydride catalysts used for hydrogen generation is tabulated in Table 1. MXene is promising for photocatalytic hydrogen production. $Ti_3AlC_2/TiO_2/Ni_2P$ was reported for photocatalytic hydrogen generation [27]. The Ni_2P cocatalyst integrated with the 2D Ti_3AlC_2/TiO_2 composite exhibited improved visible light absorption and better charge carrier separation. The 2D $Ti_3AlC_2/TiO_2/Ni_2P$ composite offered a maximum hydrogen generation of 13,000 $\mu mol \cdot g^{-1}$. It showed improved values surpassing TiO_2/Ti_3AlC_2, TiO_2/Ni_2P, and pure TiO_2 by factors of 1.29, 3.63, and 3.80, respectively [27]. $Ti_3C_2T_x$ MXene was effectively utilized as a precursor for synthesizing C-TiO_2/g-C_3N_4 photocatalysts without additional carbon, resulting in significantly enhanced hydrogen generation with HGR of 1409 $\mu mol \cdot h^{-1} \cdot g^{-1}$ [50]. It exhibited enhanced HGR of 8 times and 24 times higher than the HGR of pure g-C_3N_4 and C-TiO_2, respectively. $Ti_3C_2T_x$-supported PrF_3 nanosheets

enhanced the dehydrogenation rates of AlH_3 at low temperatures [25]. $Ti_3C_2T_x$ containing 1% of PrF_3 nanosheets showed a dehydrogenation capacity of 8.6% at 120 °C in 1.5 h, representing 93% of the calculated hydrogen capacity of used AlH_3 [25]. Ball-milling synthesized accordion-like V_2C Mxene-doped compounds in α-AlH_3 [51]. V_2C (1 wt.%)/α-AlH_3 offered superior dehydrogenation at a low temperature of 70.5 °C with a hydrogen release capacity of 8.1 wt.%. It provided 7.8 wt.% of hydrogen within 15 min at 120 °C [51]. VF_4@$Ti_3C_2T_x$ improved the dehydrogenation and rehydrogenation kinetics of $Mg(BH_4)_2$ [38]. The hydrogen gas release was observed at 90 °C using VF_4 (20 wt.%)@$Ti_3C_2T_x$ [38]. The authors reported 8.3 wt.% higher hydrogen desorption at 275 °C [38]. A palladium-doped cryo-MXene catalyst was synthesized via a wet impregnation method [39]. After HF etching, $Ti_3C_2T_x$ MXene was dropped into liquid nitrogen and kept for about 25 min at −160 °C to increase lamellar spacing, denoted as *cryo*-MXene. It was used for hydrogen generation via the hydrolysis of methylamine-borane. It offered a HGR of 159.4 min^{-1} at 318 K [39]. The hydrolysis of AB was catalyzed over $Pt_yCo_{1-y}/Ti_3C_2T_x$ [44]. $Pt_yCo_{1-y}/Ti_3C_2T_x$ showed a HGR value of 100.7 L_{H2} $(min\ g_{Pt})^{-1}$ [44]. The catalysts can be recycled based on separation via external magnets. Based on the experimental setup, hydrogen generation occurs during the in situ reduction of platinum and cobalt salts. The HGR was also calculated based on Pt. Precious metal ruthenium (Ru)-decorated TiO_2 nanospheres/$Ti_3C_2T_x$ were reported to catalyze the hydrolysis of $NaBH_4$ [46]. Spherical aberration-corrected TEM analysis revealed the homogenous dispersion of Ru nanoparticles (2 nm) over TiO_2. The catalyst with Ru (0.33 wt.%) loading demonstrated high catalytic efficacy in the hydrolysis of $NaBH_4$, achieving a hydrolysis rate of 60 $L{\cdot}min^{-1}{\cdot}g_{Ru}{}^{-1}$ at 303 K [46]. The catalyst offered high HGRs but was expensive because it used precious metals such as Ru. In conclusion, the photocatalytic hydrolysis of $NaBH_4$ using Ti_3AlC_2 is promising for further investigation in comparison with other catalysts, including MOFs [52,53], zeolitic imidazolate frameworks [54], and ZnO [55] (Table 1). The hydrolysis of $NaBH_4$ is not limited to hydrogen production but can be further used for water treatment via pollutant catalytic reduction [56–58].

Table 1. Summary of materials used for hydrogen generation via hydride hydrolysis.

Catalysts	Synthesis	Hydrogen Source	HGR	Reaction Conditions	Ref.
Pd@*cryo*-MXene	1. HF etching 2. Cryo-treatment 3. Reduction with $NaBH_4$	CH_3NH_2-BH_3	159.4 min^{-1}	50 mg of catalyst; 23 mg MeAB; 318 K	[39]
$Pt_yCo_{1-y}/Ti_3C_2T_x$	In situ reduction of Pt and Co	NH_3BH_3	100.7 L H_2 $(min\ g_{Pt})^{-1}$	10 mg of $Ti_3C_2T_x$; 0.115 mL of H_2PtCl_6 aqueous solution and $CoCl_2$; AB (34.2 mg); 318 K	[44]
$Ru/TiO_2/Ti_3C_2T_x$	1. HF etching 2. Hydrothermal method, 9 h at 90 °C 3. Settling for 24 h_4 4. Reduction with 5% hydrogen/argon mixture for 4 h at 573 K	$NaBH_4$	60 $L{\cdot}min^{-1}{\cdot}g_{Ru}{}^{-1}$	0.1 g of catalyst; 5 wt.% NaOH; 1.5 wt.% $NaBH_4$ solution; Ru loading 0.33 wt.%; 303 K	[46]
Cerium-based MOF	Hydrothermal method		1800 $mL_{H2}{\cdot}g_{cat}{}^{-1}{\cdot}min^{-1}$	50 mg catalyst; 1 g $NaBH_4$; 333 K	[52]
ZnO	Sol–gel method		3000 $mL_{H2}{\cdot}g_{cat}{}^{-1}{\cdot}min^{-1}$	10 mg catalyst; 1 wt.% $NaBH_4$; 303 K	[55]
Ti_3AlC_2/Ti_3C_2	HF etching Ultrasonication		200–300 $mL_{H2}{\cdot}g_{cat}{}^{-1}{\cdot}min^{-1}$	100 mg catalyst; 0.2 wt.%$NaBH_4$; 298 K, UV-light	Herein

3. Experimental Section

3.1. Materials and Methods

Ti_3AlC_2 (purity $\geq$ 99%, and 40–60 µm particle size) was purchased from Advanced 2D Materials CO., Ltd., Store (China). $NaBH_4$ was obtained from Sigma Aldrich (Germany).

3.2. Synthesis of $Ti_3C_2T_x$ MXene

$Ti_3C_2T_x$ was synthesized via chemical etching of Ti_3AlC_2 (0.5 g) in 30 mL of hydrofluoric acid solution (49%) for stirring at room temperature for 24 h [47]. The material was left for settling. It was separated and washed with water. It was redispered in water via ultrasonication until the formation of a stable colloid.

3.3. Material Characterization

XRD pattern was performed with a Philips PW1700 diffractometer (Philips, The Netherlands). The surface morphology of the catalyst samples was analyzed using ThermoFisher (USA, Quattro S Felid Emission Gun). It was also analyzed using TEM and HR-TEM with JSM-2100 (JOEL, Japan). DRS spectra were recorded using an Evolution 220 spectrophotometer (Thermo Fisher Scientific, UK), covering the wavelength range of 220 to 800 nm. FT-IR spectrum was obtained using a Nicolet model 6700 spectrophotometer (Thermo Fisher, USA) in the 400–4000 cm^{-1} range.

3.4. Hydrogen Generation Measurements

A 50 mL sealed photoelectrochemical cell (Corrtest®, Wuhan, China) was used to perform the catalytic reaction for $NaBH_4$ hydrolysis. 1 mL of MXene dispersion (10 mg) was added to water (50 mL) containing 0.2 g of $NaBH_4$. The reaction was performed at ambient temperature (25 $\pm$ 2 °C). The volume of hydrogen gas was measured using a water displacement method. The reaction was performed without and under UV-LED light (25 W, 365 nm, NICHIA, Japan).

After each cycle, the materials were recycled by adding 0.2 g of $NaBH_4$ to the reaction cycle. The reaction was performed using the same procedure mentioned above.

4. Conclusions

This work illustrates the efficacy of Ti_3AlC_2 MAX/Mxene multilayers as catalysts for hydrogen production via photocatalytic $NaBH_4$ hydrolysis. Light radiation can enhance HGR over time. The 2D MAX phase structure of the catalyst significantly enhanced its catalytic activity, facilitating hydrogen production at ambient temperature. The catalyst demonstrated exceptional stability and recyclability, preserving its efficacy across numerous cycles. The results underscore the significant potential of Ti_3AlC_2 MAX/MXene multilayers for practical applications in hydrogen fuel cell technology. The capacity to produce hydrogen at low temperatures and ambient settings presents considerable benefits for energy efficiency and system architecture. Continued research and development in this domain may facilitate commercializing efficient and sustainable hydrogen production techniques using MAX/MXene-based photocatalysts.

Funding: This work was supported and funded by the Deanship of Scientific Research at Imam Mohammad Ibn Saud Islamic University (IMSIU) (grant number IMSIU-DDRSP2503).

Data Availability Statement: Data is available upon reasonable request.

Conflicts of Interest: The author declare no conflict of interest.

References

1. Sazali, N. Emerging technologies by hydrogen: A review. *Int. J. Hydrogen Energy* **2020**, *45*, 18753–18771. [CrossRef]
2. Abdelhamid, H.N. A review on hydrogen generation from the hydrolysis of sodium borohydride. *Int. J. Hydrogen Energy* **2021**, *46*, 726–765. [CrossRef]
3. Kumar, A. (Ed.) *Towards Sustainable and Green Hydrogen Production by Photocatalysis: Insights into Design and Development of Efficient Materials (Volume 2)*; ACS Symposium Series; American Chemical Society: Washington, DC, USA, 2024; Volume 1468, ISBN 9780841296701.
4. David Gaima Kafadi, A.; Yusuf Hafeez, H.; Mohammed, J.; Ndikilar, C.E.; Suleiman, A.B.; Isah, A.T. A recent prospective and progress on MXene-based photocatalysts for efficient solar fuel (hydrogen) generation via photocatalytic water-splitting. *Int. J. Hydrogen Energy* **2024**, *53*, 1242–1258. [CrossRef]
5. Thabet, S.M.; Abdelhamid, H.N.; Ibrahim, S.A.; El-Bery, H.M. Boosting photocatalytic water splitting of TiO_2 using metal (Ru, Co, or Ni) co-catalysts for hydrogen generation. *Sci. Rep.* **2024**, *14*, 10115. [CrossRef]
6. Shiva Kumar, S.; Lim, H. An overview of water electrolysis technologies for green hydrogen production. *Energy Rep.* **2022**, *8*, 13793–13813. [CrossRef]
7. Onajah, S.; Sarkar, R.; Islam, M.S.; Lalley, M.; Khan, K.; Demir, M.; Abdelhamid, H.N.; Farghaly, A.A. Silica-Derived Nanostructured Electrode Materials for ORR, OER, HER, CO 2 RR Electrocatalysis, and Energy Storage Applications: A Review. *Chem. Rec.* **2024**, *24*, e202300234. [CrossRef]
8. Teli, A.M.; Mane, S.M.; Mishra, R.K.; Jeon, W.; Shin, J.C. Unveiling the Electrocatalytic Performances of the Pd-MoS2 Catalyst for Methanol-Mediated Overall Water Splitting. *Inorganics* **2025**, *13*, 21. [CrossRef]
9. Akhlaghi, N.; Najafpour-Darzi, G. A comprehensive review on biological hydrogen production. *Int. J. Hydrogen Energy* **2020**, *45*, 22492–22512. [CrossRef]
10. Páez-López, R.D.; Gómez-Soto, M.Á.; Cortés-Hernández, H.F.; Solano-Peralta, A.; Castro, M.; Kroneck, P.M.H.; Sosa-Torres, M.E. Understanding Dioxygen Activation in the Fe(III)-Promoted Oxidative Dehydrogenation of Amines: A Computational Study. *Inorganics* **2025**, *13*, 22. [CrossRef]
11. Holladay, J.D.; Hu, J.; King, D.L.; Wang, Y. An overview of hydrogen production technologies. *Catal. Today* **2009**, *139*, 244–260. [CrossRef]
12. Saleh, M.; Abdelhamid, H.N.; Fouad, D.M.; El-Bery, H.M. Enhancing photocatalytic water splitting: Comparative study of TiO_2 decorated nanocrystals (Pt and Cu) using different synthesis methods. *Fuel* **2023**, *354*, 129248. [CrossRef]
13. Davis Cortina, M.; Romero de Terreros Aramburu, M.; Neves, A.M.; Hurtado, L.; Jepsen, J.; Ulmer, U. The Integration of Thermal Energy Storage Within Metal Hydride Systems: A Comprehensive Review. *Inorganics* **2024**, *12*, 313. [CrossRef]
14. Abdelhamid, H.N. Salts Induced Formation of Hierarchical Porous ZIF-8 and Their Applications for CO_2 Sorption and Hydrogen Generation via NaBH4 Hydrolysis. *Macromol. Chem. Phys.* **2020**, *221*, 2000031. [CrossRef]
15. Abdelhamid, H.N. Hierarchical porous ZIF-8 for hydrogen production via the hydrolysis of sodium borohydride. *Dalt. Trans.* **2020**, *49*, 4416–4424. [CrossRef] [PubMed]
16. Gogotsi, Y. *MXenes*; Jenny Stanford Publishing: New York, NY, USA, 2023; ISBN 9781003306511.
17. Li, X.; Huang, Z.; Shuck, C.E.; Liang, G.; Gogotsi, Y.; Zhi, C. MXene chemistry, electrochemistry and energy storage applications. *Nat. Rev. Chem.* **2022**, *6*, 389–404. [CrossRef] [PubMed]
18. Amara, U.; Hussain, I.; Ahmad, M.; Mahmood, K.; Zhang, K. 2D MXene-Based Biosensing: A Review. *Small* **2023**, *19*, 2205249. [CrossRef]
19. Cao, W.; Nie, J.; Cao, Y.; Gao, C.; Wang, M.; Wang, W.; Lu, X.; Ma, X.; Zhong, P. A review of how to improve Ti_3C_2Tx MXene stability. *Chem. Eng. J.* **2024**, *496*, 154097. [CrossRef]
20. Isa, A.T.; Hafeez, H.Y.; Mohammed, J.; Ndikilar, C.E.; Suleiman, A.B.; Kafadi, A.D.G. Photocatalytic performance of MXenes cocatalyst in hydrogen (H_2) production via photocatalytic water splitting: A review. *J. Alloys Compd.* **2024**, *1005*, 175951. [CrossRef]
21. Tie, L.; Li, N.; Yu, C.; Liu, Y.; Yang, S.; Chen, H.; Dong, S.; Sun, J.; Dou, S.; Sun, J. Self-Supported Nonprecious MXene/Ni_3S_2 Electrocatalysts for Efficient Hydrogen Generation in Alkaline Media. *ACS Appl. Energy Mater.* **2019**, *2*, 6931–6938. [CrossRef]
22. Thirumal, V.; Yuvakkumar, R.; Kumar, P.S.; Ravi, G.; Arun, A.; Guduru, R.K.; Velauthapillai, D. Heterostructured two dimensional materials of MXene and graphene by hydrothermal method for efficient hydrogen production and HER activities. *Int. J. Hydrogen Energy* **2023**, *48*, 6478–6487. [CrossRef]
23. Sanna, M.; Ng, S.; Vaghasiya, J.V.; Pumera, M. Fluorinated MAX Phases for Photoelectrochemical Hydrogen Evolution. *ACS Sustain. Chem. Eng.* **2022**, *10*, 2793–2801. [CrossRef]
24. Tahir, M.; Mansoor, R. Constructing a stable 2D Ti_3AlC_2 MnAXm cocatalyst-modified gC_3N_4/CoAl-LDH/Ti_3AlC_2 heterojunction for efficient dry and bireforming of methane for photocatalytic syngas production. *J. Alloys Compd.* **2023**, *947*, 169457. [CrossRef]
25. Liang, L.; Zhao, S.; Wang, C.; Yin, D.; Wang, S.; Wang, Q.; Liang, F.; Li, S.; Wang, L.; Cheng, Y. Heterojunction synergistic catalysis of MXene-supported PrF3 nanosheets for the efficient hydrogen storage of AlH_3. *Nano Res.* **2023**, *16*, 9546–9552. [CrossRef]

26. Biswal, L.; Mohanty, R.; Nayak, S.; Parida, K. Review on MXene/TiO_2 nanohybrids for photocatalytic hydrogen production and pollutant degradations. *J. Environ. Chem. Eng.* **2022**, *10*, 107211. [CrossRef]
27. Tasleem, S.; Tahir, M.; Zakaria, Z.Y. Fabricating structured 2D Ti_3AlC_2 MAX dispersed TiO_2 heterostructure with Ni_2P as a cocatalyst for efficient photocatalytic H2 production. *J. Alloys Compd.* **2020**, *842*, 155752. [CrossRef]
28. Yang, J.-X.; Yu, W.-B.; Li, C.-F.; Dong, W.-D.; Jiang, L.-Q.; Zhou, N.; Zhuang, Z.-P.; Liu, J.; Hu, Z.-Y.; Zhao, H.; et al. PtO nanodots promoting Ti_3C_2 MXene in-situ converted Ti_3C_2/TiO_2 composites for photocatalytic hydrogen production. *Chem. Eng. J.* **2021**, *420*, 129695. [CrossRef]
29. Sun, B.; Qiu, P.; Liang, Z.; Xue, Y.; Zhang, X.; Yang, L.; Cui, H.; Tian, J. The fabrication of 1D/2D CdS nanorod@Ti_3C_2 MXene composites for good photocatalytic activity of hydrogen generation and ammonia synthesis. *Chem. Eng. J.* **2021**, *406*, 127177. [CrossRef]
30. Wang, Y.; Wang, X.; Ji, Y.; Bian, R.; Li, J.; Zhang, X.; Tian, J.; Yang, Q.; Shi, F. Ti_3C_2 MXene coupled with CdS nanoflowers as 2D/3D heterostructures for enhanced photocatalytic hydrogen production activity. *Int. J. Hydrogen Energy* **2022**, *47*, 22045–22053. [CrossRef]
31. Zeng, H.; Li, Z.; Li, G.; Cui, X.; Jin, M.; Xie, T.; Liu, L.; Jiang, M.; Zhong, X.; Zhang, Y.; et al. Interfacial Engineering of TiO_2/Ti_3C_2 MXene/Carbon Nitride Hybrids Boosting Charge Transfer for Efficient Photocatalytic Hydrogen Evolution. *Adv. Energy Mater.* **2022**, *12*, 2102765. [CrossRef]
32. Ye, X.; Zhong, H.; Zhang, Y.; Liu, X.; Tian, W.; Ma, L.-A.; Wang, Q. Ti_3C_2 MXene cocatalyst supported $Ti_3C_2/SrTiO_3/g\text{-}C_3N_4$ heterojunctions with efficient electron transfer for photocatalytic H_2 production. *CrystEngComm* **2024**, *26*, 5440–5451. [CrossRef]
33. Fattah-alhosseini, A.; Sangarimotlagh, Z.; Karbasi, M. Latest progress in photocatalytic hydrogen production using MXene (Ti_3C_2)/MOFs composite: A review. *Int. J. Hydrogen Energy* **2024**, *79*, 771–790. [CrossRef]
34. Chen, Y.; Zhu, H.; Kang, S.-Z.; Zhang, T.; Qin, L.; Li, X. Facilely in-situ growth of porphyrin metal-organic frameworks on the Ti_3C_2 MXene/TiO_2 for greatly improved photocatalytic hydrogen generation. *J. Alloys Compd.* **2023**, *961*, 170929. [CrossRef]
35. Su, T.; Hood, Z.D.; Naguib, M.; Bai, L.; Luo, S.; Rouleau, C.M.; Ivanov, I.N.; Ji, H.; Qin, Z.; Wu, Z. Monolayer Ti_3C_2Tx as an Effective Cocatalyst for Enhanced Photocatalytic Hydrogen Production over TiO_2. *ACS Appl. Energy Mater.* **2019**, *2*, 4640–4651. [CrossRef]
36. Mistry, K.; Lakhani, R.; Tripathi, B.; Shinde, S.; Chandra, P. Recent trends in MXene/Metal chalcogenides for electro-/photocatalytic hydrogen evolution reactions. *Int. J. Hydrogen Energy* **2022**, *47*, 41711–41732. [CrossRef]
37. Ghotia, S.; Kumar, A.; Sudarsan, V.; Dwivedi, N.; Singh, S.; Kumar, P. Multilayered Ti_3C_2Tx MXenes: A prominent materials for hydrogen storage. *Int. J. Hydrogen Energy* **2024**, *52*, 100–107. [CrossRef]
38. Zhang, Z.; Gao, D.; Zheng, J.; Xia, A.; Zhang, Q.; Wang, L.; Zhang, L. Heterostructured VF4@Ti_3C_2 catalyst improving reversible hydrogen storage properties of $Mg(BH4)_2$. *Chem. Eng. J.* **2023**, *460*, 141690. [CrossRef]
39. Karataş, Y.; Çetin, T.; Akinay, Y.; Gülcan, M. Synthesis and characterization of Pd doped MXene for hydrogen production from the hydrolysis of methylamine borane: Effect of cryogenic treatment. *J. Energy Inst.* **2023**, *109*, 101310. [CrossRef]
40. Liu, X.; Chen, W.; Zhang, X. Ti_3AlC_2/Pd Composites for Efficient Hydrogen Production from Alkaline Formaldehyde Solutions. *Nanomaterials* **2022**, *12*, 843. [CrossRef]
41. Yao, F.; Guan, S.; Bian, L.; Fan, Y.; Liu, X.; Zhang, H.; Li, B.; Liu, B. Ensemble-Exciting Effect in Pd/alk-Ti_3C_2 on the Activity for Efficient Hydrogen Production. *ACS Sustain. Chem. Eng.* **2021**, *9*, 12332–12340. [CrossRef]
42. Liang, L.; Bian, L.; Fan, Y.; Guan, S.; Liu, X.; Sun, Q.; Liu, B. Nitrogen doping excited Ru and Ti_3C_2-xNx support for hydrogen generation from ammonia borane. *Fuel* **2023**, *339*, 127445. [CrossRef]
43. Slot, T.K.; Yue, F.; Xu, H.; Ramos-Fernandez, E.V.; Sepúlveda-Escribano, A.; Sofer, Z.; Rothenberg, G.; Shiju, N.R. Surface oxidation of Ti_3C_2Tx enhances the catalytic activity of supported platinum nanoparticles in ammonia borane hydrolysis. *2F Mater.* **2020**, *8*, 015001. [CrossRef]
44. Fan, G.; Li, X.; Ma, Y.; Zhang, Y.; Wu, J.; Xu, B.; Sun, T.; Gao, D.; Bi, J. Magnetic, recyclable $PtyCo1-y/Ti_3C_2X_2$ (X = O, F) catalyst: A facile synthesis and enhanced catalytic activity for hydrogen generation from the hydrolysis of ammonia borane. *New J. Chem.* **2017**, *41*, 2793–2799. [CrossRef]
45. Guo, F.; Zou, H.; Yao, Q.; Huang, B.; Lu, Z.-H. Monodispersed bimetallic nanoparticles anchored on TiO_2-decorated titanium carbide MXene for efficient hydrogen production from hydrazine in aqueous solution. *Renew. Energy* **2020**, *155*, 1293–1301. [CrossRef]
46. Li, T.; Xiang, C.; Chu, H.; Xu, F.; Sun, L.; Zou, Y.; Zhang, J. Catalytic effect of highly dispersed ultrafine Ru nanoparticles on a TiO_2-Ti_3C_2 support: Hydrolysis of sodium borohydride for H2 generation. *J. Alloys Compd.* **2022**, *906*, 164380. [CrossRef]
47. Alhabeb, M.; Maleski, K.; Anasori, B.; Lelyukh, P.; Clark, L.; Sin, S.; Gogotsi, Y. Guidelines for Synthesis and Processing of Two-Dimensional Titanium Carbide (Ti_3C_2Tx MXene). *Chem. Mater.* **2017**, *29*, 7633–7644. [CrossRef]
48. Xu, Y.; Wang, S.; Yang, J.; Han, B.; Nie, R.; Wang, J.; Wang, J.; Jing, H. In-situ grown nanocrystal TiO_2 on 2D Ti_3C_2 nanosheets for artificial photosynthesis of chemical fuels. *Nano Energy* **2018**, *51*, 442–450. [CrossRef]

49. Gao, Y.; Wang, L.; Zhou, A.; Li, Z.; Chen, J.; Bala, H.; Hu, Q.; Cao, X. Hydrothermal synthesis of TiO_2/Ti_3C_2 nanocomposites with enhanced photocatalytic activity. *Mater. Lett.* **2015**, *150*, 62–64. [CrossRef]
50. Han, X.; An, L.; Hu, Y.; Li, Y.; Hou, C.; Wang, H.; Zhang, Q. Ti3C2 MXene-derived carbon-doped TiO_2 coupled with g-C_3N_4 as the visible-light photocatalysts for photocatalytic H2 generation. *Appl. Catal. B Environ.* **2020**, *265*, 118539. [CrossRef]
51. Lin, Z.; Yuan, Z.; Zhang, H.; Guan, S.; Wang, X.; Zhao, S.; Fan, G.; Fan, Y.; Liu, B. Excellent catalytic effect of V2C MXene on dehydrogenation performance of α-AlH3. *Int. J. Hydrogen Energy* **2024**, *56*, 998–1006. [CrossRef]
52. Hussein Hashem, Z.; Abdel-Rahman, L.H.; Gómez-Ruiz, S.; Abdelhamid, H.N. Cerium-Organic Framework (CeOF) for hydrogen generation via the hydrolysis of $NaBH_4$. *Results Chem.* **2024**, *7*, 101412. [CrossRef]
53. Saleh, M.R.; El-Bery, H.M.; Abdelhamid, H.N. Co@ZIF-8/TiO_2 Heterojunction for Green Hydrogen Generation. *Appl. Organomet. Chem.* **2022**, *37*, e6995. [CrossRef]
54. Abdelhamid, H.N. Dehydrogenation of sodium borohydride using cobalt embedded zeolitic imidazolate frameworks. *J. Solid State Chem.* **2021**, *297*, 122034. [CrossRef]
55. Althubiti, N.A.; Taha, T.A.; Azab, A.A.; Abdelhamid, H.N. ZnO-based nanocomposites for hydrogen generation via hydrolysis of Borohydride. *J. Sol-Gel Sci. Technol.* **2023**, *106*, 837–846. [CrossRef]
56. Abdellatif, A.B.A.; El-Bery, H.M.; Abdelhamid, H.N.; El-Gyar, S.A. ZIF-67 and Cobalt-based@heteroatom–doped carbon nanomaterials for hydrogen production and dyes removal via adsorption and catalytic degradation. *J. Environ. Chem. Eng.* **2022**, *10*, 108848. [CrossRef]
57. Abdelhamid, H.N.; Mathew, A.P. In-situ growth of zeolitic imidazolate frameworks into a cellulosic filter paper for the reduction of 4-nitrophenol. *Carbohydr. Polym.* **2021**, *274*, 118657. [CrossRef]
58. Georgouvelas, D.; Abdelhamid, H.N.; Li, J.; Edlund, U.; Mathew, A.P. All-cellulose functional membranes for water treatment: Adsorption of metal ions and catalytic decolorization of dyes. *Carbohydr. Polym.* **2021**, *264*, 118044. [CrossRef]

Disclaimer/Publisher's Note: The statements, opinions and data contained in all publications are solely those of the individual author(s) and contributor(s) and not of MDPI and/or the editor(s). MDPI and/or the editor(s) disclaim responsibility for any injury to people or property resulting from any ideas, methods, instructions or products referred to in the content.